Solar RRL
www.solar-rrl.com

Quantifying Quasi-Fermi Level Splitting and Open-Circuit Voltage Losses in Highly Efficient Nonfullerene Organic Solar Cells

Le Quang Phuong, Seyed Mehrdad Hosseini, Oskar J. Sandberg,* Yingping Zou, Han Young Woo, Dieter Neher, and Safa Shoaee**

The power conversion efficiency (PCE) of state-of-the-art organic solar cells is still limited by significant open-circuit voltage (V_{OC}) losses, partly due to the excitonic nature of organic materials and partly due to ill-designed architectures. Thus, quantifying different contributions of the V_{OC} losses is of importance to enable further improvements in the performance of organic solar cells. Herein, the spectroscopic and semiconductor device physics approaches are combined to identify and quantify losses from surface recombination and bulk recombination. Several state-of-the-art systems that demonstrate different V_{OC} losses in their performance are presented. By evaluating the quasi-Fermi level splitting (QFLS) and the V_{OC} as a function of the excitation fluence in nonfullerene-based PM6:Y6, PM6:Y11, and fullerene-based PPDT2FBT:PCBM devices with different architectures, the voltage losses due to different recombination processes occurring in the active layers, the transport layers, and at the interfaces are assessed. It is found that surface recombination at interfaces in the studied solar cells is negligible, and thus, suppressing the nonradiative recombination in the active layers is the key factor to enhance the PCE of these devices. This study provides a universal tool to explain and further improve the performance of recently demonstrated high-open-circuit-voltage organic solar cells.

1. Introduction

The judicious design of nonfullerene acceptors (NFAs) have brought organic solar cells (OSCs) back to the race with other emerging photovoltaic materials for advancing alternative techniques to harvest more efficient solar energy.[1–5] Single-junction OSCs containing a blend of NFAs and donor polymers have achieved state-of-the-art power conversion efficiencies (PCEs) of 18.2%.[6] The short-circuit (SC) current J_{SC} of NFA OSCs is well enhanced to reach a value near 28 mA cm^{-2} due to additional absorption in the near-infrared spectral region of small-molecule NFAs[4–6] and efficient free charge generation.[7] To reach their theoretical maximum efficiency, improvement in solar cell efficiency now really relies upon achieving higher open-circuit voltages (V_{OC}). In this regard, many researchers have used the detailed balance theory to quantify the nonradiative and radiative voltage losses in OSCs.[8] Despite the improvements in reducing voltage losses in state-of-the-art low-offset OSCs, a relatively large nonradiative recombination still remains at the heart of the loss in V_{OC}.[9–13]

Dr. L. Q. Phuong, S. M. Hosseini, Prof. S. Shoaee
Optoelectronics of Disordered Semiconductors
Institute of Physics and Astronomy
University of Potsdam
Karl-Liebknecht-Straße 24-25, Potsdam-Golm 14476, Germany
E-mail: phuonglq28@gmail.com; shoai@uni-potsdam.de

Prof. D. Neher
Soft Matter Physics and Optoelectronics
Institute of Physics and Astronomy
University of Potsdam
Karl-Liebknecht-Straße 24-25, Potsdam-Golm 14476, Germany

The ORCID identification number(s) for the author(s) of this article can be found under https://doi.org/10.1002/solr.202000649.

DOI: 10.1002/solr.202000649

Dr. O. J. Sandberg
Sustainable Advanced Materials
Department of Physics
Swansea University
Singleton Park
Swansea SA2 8PP, Wales, UK
E-mail: o.j.sandberg@swansea.ac.uk

Prof. Y. Zou
College of Chemistry and Chemical Engineering
Central South University
Changsha 410083, P. R. China

Prof. H. Y. Woo
Department of Chemistry
College of Science
Korea University
145 Anam-ro, Seongbuk-gu, Seoul 02841, Republic of Korea

Thus to achieve the full potential of NFA-based solar cells, it is imperative to suppress all nonradiative recombination losses. Recombination losses can occur either in the bulk [singlet and/or triplet charge transfer (CT) states] or across the interface of an interlayer between charges in the transport layer and minority carriers in the absorbing layer.[14–19] As such, understanding the source of the different channels and contribution to nonradiative recombination is of paramount importance.[20] However, one of the most difficult tasks in identifying the origin behind the voltage loss in OSCs under practical operation is the appropriate quantification of quasi-Fermi level splitting (QFLS) in OSCs. The QFLS concept, which was originally proposed by Shockley,[21] is a standard construct for describing the operation of semiconductor electronic, optoelectronic, and electrochemical devices. In the Shockley–Queisser theory, the QFLS and the voltage at any light intensity are two interchangeable quantities, which are considered as equal to each other. Because of the direct relationship with charge transport processes in nanoscale junctions, there have been also intensive ongoing efforts to explicitly measure the QFLS. The QFLS demonstrates an internal quantity of active material, whereas the V_{OC} reflects an external quantity, measured at external electrodes.[22–24] So thermodynamically, the QFLS represents the maximum V_{OC} a solar cell can achieve. Thus, the difference between the V_{OC} and the QFLS is correlated with recombination losses occurring in the charge transporting layers and at interfaces.[25] In addition, nonradiative recombination in bulk and at the surface of the absorbing layer leads to a deviation of the QFLS from the radiative limit QFLS. In material systems where the photoluminescence (PL) mostly stems from the recombination of free carriers, such as perovskites and GaAs, transient PL and PL quantum yield have been exploited widely to evaluate the QFLS in various sample architectures.[26–29] However, these techniques when applied to OSCs are rather challenging. The central challenge is that organic materials are excitonic systems,[30] where upon absorption of light the primary species that is formed is a Coulombically bound electron–hole pair called a singlet exciton, which can decay radiatively to the ground state—manifested as fluorescence. Even in the scenario of exciton dissociation, a ≈0.1% residual of the exciton remains, which has a strong radiative contribution compared with any other radiative events. In addition, the current picture of the organic photovoltaic operation focuses on free charge generation and subsequent recombination occurring through manifold CT states formed at the interface between electron donor and acceptor phases.[31] The decay of which regenerates a neutral ground state, a process mostly being nonradiative in nature,[32] as the CT states are very weakly luminescent.[33] Thereby, the PL data of OSCs will not yield all the information required and generally consist of components originating predominantly from the singlet excitons and to a much lesser extent from the CT excitons. This is particularly the case in low-offset donor–acceptor systems, where singlet excitons and CT states can concurrently occur.

In this work, we use quasi-steady-state photoinduced absorption (PIA) spectroscopy to evaluate directly the QFLS based on experimental data on carrier generation and recombination. We study PM6:Y6, PM6:Y11, and PPDT2FBT:PCBM systems and compare the evolution of the QFLS and the V_{OC} of the very same device over a range of excitation fluences. In the studied systems, the calculated QFLS is very close to the V_{OC} values, which do not saturate with fluence. Thus, we exclude photoinduced self-heating and temperature-related effects and furthermore, we identify that the voltage losses due to recombination across the transport layers and at the interfaces are negligible in optimum devices. However, upon removing the transport layers in PM6:Y6, surface recombination becomes significant and causes a noticeable voltage loss of about 450 mV. Thus, the main voltage loss in the optimum device configuration is caused by the radiative and nonradiative recombination in the absorbing layer. This implies that for improving V_{OC} in the optimum PM6:Y6 device, charge carrier recombination within the bulk has to be reduced, rather than recombination at the interfaces (in contrast to perovskite cells).

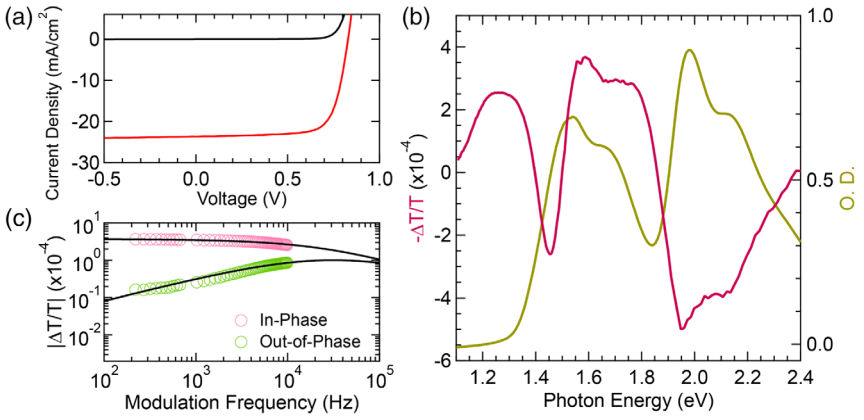

Figure 1. a) *J–V* curves of a semitransparent PM6:Y6 device measured in the dark (black curve) and under simulated AM 1.5G illumination (red curve). b) The PIA and absorption spectra of a semitransparent PM6:Y6 device. c) The in-phase and out-of-phase components of the 1.25-eV PIA peak of a semitransparent PM6:Y6 device under illumination equivalent to 1 sun at OC condition as a function of the modulation frequency. The solid curves show the global fitting curves using the equation described in Supporting Information. The average lifetime of free carriers at the OC condition is estimated to be about 5 µs.

2. Results and Discussion

Figure 1a shows typical J–V curves of the PM6:Y6 (semitransparent) device measured in the dark and under simulated AM1.5G illumination. The semitransparent device exhibits an average PCE of 14.4% (the optimum PCE is 15%) with a V_{OC} of 0.83 V, a J_{SC} of 23.3 mA cm^{-2}, and a fill factor (FF) of 0.73. A schematic of the energetics of the full device architecture and the calculated J_{SC} from the external quantum efficiency (EQE) spectrum is shown in Figure S1, Supporting Information. To probe the recombination dynamics we use quasi-steady-state PIA.[34,35] We have previously demonstrated that high-sensitivity PIA can be used to monitor the yield and the dynamics of free carriers.[36] This technique overcomes many issues other charge extraction techniques can encounter and as such provides a reliable platform for conducting recombination studies (full experimental details are given in the Supporting Information). PIA and the absorption spectra of the semitransparent PM6:Y6 device and film, respectively are shown in Figure 1b. Two photobleaching peaks emerge near the band-edge absorptions of PM6 (1.95 eV) and Y6 (1.45 eV), and broad PIA bands peaking at 1.25, 1.6, and 1.8 eV appear in the PIA spectrum. The excitations responsible for the PIA peak at 1.25 eV have an average lifetime τ of 5 μs in PM6:Y6 device at the open-circuit (OC) condition under illumination equivalent to 1 sun (producing the same J_{SC} under simulated AM1.5G illumination), as shown in Figure 1c. This is in line with reported lifetimes of charge carriers in various organic semiconductors.[36] The PIA peaks at higher energies have lifetimes beyond the time resolution of the measurement system (Figure S2, Supporting Information). Moreover, given that the 1.25-eV PIA band is still present when changing Y6 to another acceptor, namely Y11 (Figure S3, Supporting Information), we assign this PIA band to the absorption of free holes in PM6. Note that as the higher PIA bands separate spectrally from the 1.25-eV PIA band and a sharp photobleaching band emerging near the band edge of Y6 locates between the PIA bands, the higher-energy PIA bands do not affect the 1.25-eV PIA band's intensity.

In order to get the QFLS, the PIA signal has to be translated to the excess carrier concentration in the device, by first evaluating the absorption cross section σ of the free carriers. This is achieved by considering the PIA signal and the photocurrent both under the SC condition (Figure S4, Supporting Information). It should be noted that the PIA probes the average density of the holes in the bulk of the active layer. While we cannot make an assumption on the excess electron carrier density, however, the extraction of the carriers has to be balanced under steady-state conditions $\mu_e n_{sc} = \mu_h p_{sc}$, where μ_h (μ_e) is the hole (electron) mobility and p_{sc} (n_{sc}) is the average excess hole (electron) concentration over the device under the SC condition (see Supporting Information for the derivation). J_{SC} is thus expressed in terms of the average excess hole concentration as

$$J_{sc} = 2q\mu_h p_{sc}|F| = 2q\mu_h p_{sc}\frac{V_{bi}}{d} \quad (1)$$

where q is the elementary charge, F is the electric field in the device, d is the active layer thickness, and V_{bi} is the built-in potential. Substituting $p_{sc} = \frac{PIA_{sc}}{\sigma d}$ into Equation (1), where PIA_{SC} is the PIA signal under the SC condition, we obtain

$$\frac{\mu_h}{\sigma} = \frac{J_{sc}d^2}{2qV_{bi}PIA_{sc}} \quad (2)$$

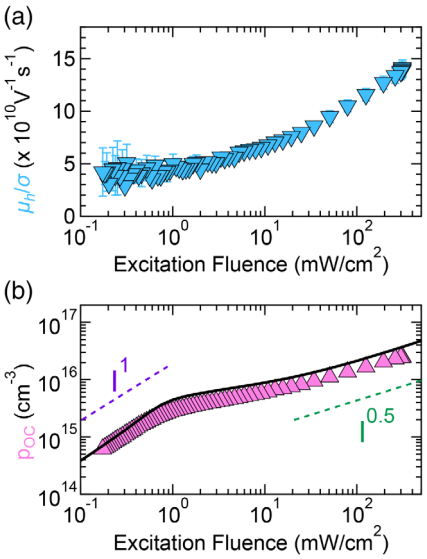

Figure 2. a) μ_h/σ derived from the J_{SC} and the PIA_{SC} data as described in the main text. b) The excess hole concentration p_{oc} at the OC condition as a function of the excitation fluence. The solid curve shows a simulated result of a drift-diffusion simulation. The dashed lines are guides for the eye.

Figure 2a shows a plot of $\frac{\mu_h}{\sigma}$ as a function of the excitation fluence I_{ex} for the PM6:Y6 device. The product $\frac{\mu_h}{\sigma}$ is rather constant at low fluences and gradually increases with increasing I_{ex}. Such dependence of the carrier mobility on I_{ex} has been evidenced widely in amorphous and semiconducting organic materials.[37] The steady-state space–charge-limited current (SCLC) measurement for hole-only diodes yields $\mu_h = 6.5 \times 10^{-5}$ cm^2 Vs^{-1} (Figure S6, Supporting Information), from which the absorption cross section σ of free carriers in the PM6:Y6 device is estimated to be 1.54×10^{-15} cm^2, which is in agreement with σ values observed for other organic semiconductors.[36,38,39] It is worth mentioning here that this SCLC mobility is not responsible for the FF of the device measured under 1 sun illumination. As shown in Figure 2a, the carrier mobility under illumination comparable with 1 sun condition becomes roughly three times larger than the plateau value at low excitation fluences. And as shown later, even an error of factor 3 on the mobility leads to an error of only 28 meV in QFLS, which is less than 10% of the nonradiative and radiative losses.

Figure 2b shows excess hole concentration at the OC condition, p_{oc}, as a function of excitation fluence in the PM6:Y6 device. The excess hole density at OC is found to be 2×10^{16} cm^{-3} under excitation comparable with 1 sun. The linear excitation fluence dependence of p_{oc} at low I_{ex} indicates first-order loss in the device.[40] In contrast, the power-dependent slope of 0.5 at I_{ex} above 10 mW cm^{-2} reveals a predominant carrier loss due to nongeminate recombination. First-order and second-order rate

constants are approximated to be $5 \times 10^3\,s^{-1}$ (Figure S7, Supporting Information) and $1.07 \times 10^{-11}\,cm^3s^{-1}$, respectively. This k_2 value is similar to that determined by other charge extraction measurement techniques (Figure S8, Supporting Information). Using this experimental recombination rate, we also conduct drift-diffusion simulations[41] of the average excess hole density as a function of excitation fluence under the OC condition for the device. As shown in Figure 2b, the experimental PIA result follows quite well with the simulation. The linear p_{oc} at low intensities is due to the shunt which effectively brings the device closer toward the SC condition. On the other hand, the plateau of p_{oc} seen at moderate intensities is caused by photovoltage-induced injected carriers from the ohmic contacts; this signature can be used as an indication of ohmic (injecting) contacts.

Now with the knowledge of carrier concentration, QFLS can be expressed as[22]

$$\mathrm{QFLS} = k_B T \ln\left(\frac{np}{n_i^2}\right) \tag{3}$$

where n (p) is the excess electron (hole) concentration, k_B is the Boltzmann constant, n_i is the intrinsic carrier concentration, and T is the temperature. We evaluate n_i^2 from $\mathrm{EQE_{EL}}$, $\mathrm{EQE_{PV}}$, and k_2 data (see Figures S9 and S10, Supporting Information). Under the OC condition, by considering $n = p = p_{oc}$, we quantify the QFLS. This is shown in **Figure 3**a along with the radiative limit $\mathrm{QFLS_{Rad}}$ and qV_{OC} of the PM6:Y6 device as a function of the excitation fluence I_{ex}. The radiative limit $\mathrm{QFLS_{Rad}}$ is calculated as $\mathrm{QFLS_{Rad}} = k_B T \ln(\frac{J_{SC}}{J_0^{Rad}})$, where J_0^{Rad} is the dark radiative saturation current. It is important to note that as PIA measurement probes directly the excess carrier concentration in the active layer, which is determined by the radiative and nonradiative recombination in bulk, the QFLS reflects an internal quantity of the active layer. Meanwhile, qV_{OC} discloses an external quantity recorded at the external electrodes of the device. The majority carriers in the transport layer might be captured by the interfacial trapping centers. Moreover, when the minority carriers travel to the wrong electrode, at the interface of the active layer and the interlayer, or across the interlayer, there may be recombination with the majority carriers; this loss is termed surface recombination. Therefore, the QFLS sets the upper limit for qV_{OC} that can be reached when there are no carrier losses in the transport interlayers and at the interfaces. We first discuss the relation between the QFLS and the V_{OC} in the optimum PM6:Y6 device (with the transport interlayers), as shown in Figure 3a. The sharp increase of qV_{OC} in the low I_{ex} indicates a shunt effect.[14] This carrier leakage results in a discrepancy between the external V_{OC} and the internal QFLS in the low I_{ex} region. In contrast, at a higher I_{ex} region, the QFLS and V_{OC} experience a nearly identical excitation fluence dependence. Note that neither QFLS nor V_{OC} saturate with increasing fluence even up to ≈3 suns. The equivalent QFLS and V_{OC} imply that there is negligible recombination inside the PEDOT:PSS and/or PDINO transport layers and at the interfaces with the PM6:Y6 active layer. This conclusion is further supported by the observation of very similar excitation-fluence-dependent PIA signals/carrier concentrations of the PM6:Y6 film and the full device, where in the former bulk recombination plays the most dominant role (see Figure S11, Supporting Information). Furthermore, the behavior of each interlayer is also examined, revealing voltage losses of about 10 meV due to recombination at each interface between the active layer and the transporting layers under illumination equivalent to 1 sun, which is insignificant in comparison with the loss due to bulk recombination (Figure S12, Supporting Information). As a result, the main voltage loss in the optimized structure stems from the recombination processes in the active layer. Under 1 sun excitation, the V_{OC} loss due to the radiative recombination in the active layer is 305 meV [the difference between E_g determined as the inflection point of the EQE spectrum[42,43] (see Figure S13, Supporting Information) and the $\mathrm{QFLS_{Rad}}$]. The nonradiative recombination processes cause a further loss of 307 meV in the V_{OC} loss. These findings are confirmed by the drift-diffusion simulations. The

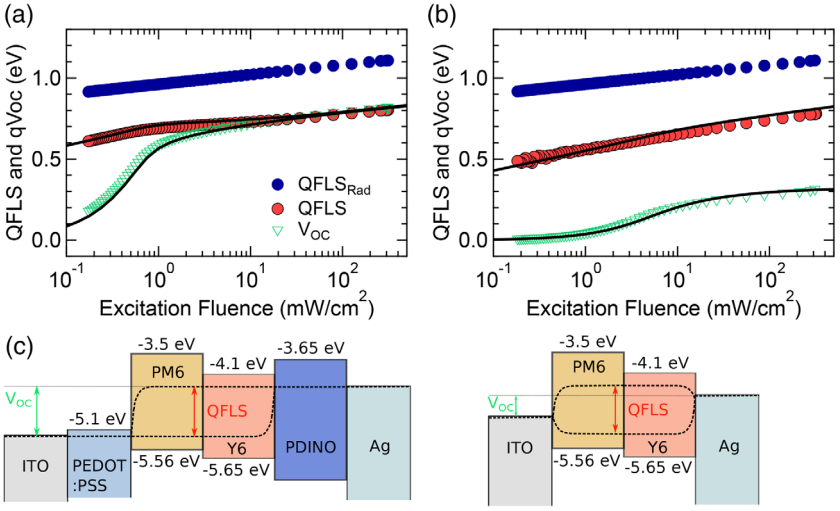

Figure 3. The excitation fluence dependences of qV_{OC}, the QFLS, and the radiative limit $\mathrm{QFLS_{Rad}}$ of the PM6:Y6 devices a) with and b) without the transport interlayers at room temperature. The black solid curves are the simulation results of the QFLS and V_{OC} data. Note that the V_{OC} data is obtained by the *J–V* scans performed under the very same excitation used in the PIA measurements, which provides the QFLS data, but not modulated. c) Schematics showing the relation between the QFLS and the V_{OC} in PM6:Y6 devices with and without the transport interlayers under 1 sun excitation.

corresponding simulated V_{OC} along with the QFLS obtained from PIA is shown in Figure 3a, as indicted by black solid curves. Again, note that the PIA, and hence QLFS from PIA, is limited by the shunt at low intensities and photovoltage-induced injection from ohmic contacts at moderate intensities. An excellent agreement between the simulations and the experimental data is obtained, not only confirming that PIA probes the average density, but also that the contacts are ohmic.

Figure 3b shows how the correlation between QFLS and V_{OC} changes when there are significant carrier losses at the interfaces, for PM6:Y6 devices fabricated without any transport interlayers. For these devices, the V_{OC} and QFLS data in the low I_{ex} region demonstrate that the shunt effect becomes more severe than that in the optimum device, which is consistent with the J–V data measured in the dark for these devices. The V_{OC} now suffers from 453 meV loss under 1 sun condition. We attribute this extra loss between the QFLS and the V_{OC} in this device to surface recombination occurred at the interfaces of the active layer with ITO and Ag electrodes. The diffusion length of carriers in 100-nm PM6:Y6 devices was recently reported to be comparable with the thickness of the active layer.[44] When the transporting layers which reduce the diffusion of the minority carriers towards the wrong electrodes are removed, the long diffusion lengths of carriers might enhance surface recombination.[45] These results are reproduced by corresponding simulations, shown by the solid black curves in Figure 3b, for a PM6:Y6 device with nonohmic contacts, exhibiting considerable injection barriers for holes at the anode and electrons at the cathode contacts, respectively. The simulations confirm that, under the OC condition, this device is influenced by surface recombination taking place at the contacts, strongly limiting the V_{OC}.[46] Moreover, as the contacts are nonohmic, the signature of injected carriers is essentially absent in the PIA. Instead, the PIA reflects the QFLS inside the bulk across the entire intensity range. Schematics describing the relation between the QFLS and the V_{OC} in devices with and without surface recombination are shown in Figure 3c. Our results clearly point out that PEDOT:PSS and PDINO transport materials are rather selective charge transport layers and sufficient for the PM6:Y6 device with respect to terminating surface recombination.

We note that our concept to identify and quantify surface recombination and bulk recombination can be successfully generalized to other systems, as demonstrated by a fullerene and another nonfullerene system (see Figure S14 and S15, Supporting Information). The methodology proposed in this work constitutes a relatively reliable approach to investigate the true nature of the recombination of charges, even in complex device architectures, providing essential information about the physics in these devices.

In addition, using this approach we quantify the nonradiative energy loss of PM6:Y6 to be 307 meV compared with 275 meV, as obtained from EQE_{EL} (by us or reported by others).[47] The discrepancy between the two values stems from the fact that in low-offset donor acceptor systems, emissive singlet excitons strongly contribute to the EQE of the CT states, thus falsifying the measured nonradiative efficiency. The correct quantification of the nonradiative voltage loss in the bulk (and across the interfaces) is critical in determining the correct V_{OC} losses in the state-of-the-art low-offset systems.

3. Conclusions

In conclusion, quasi-steady-state PIA spectroscopy allowed us to probe QFLS in OSCs to identify and quantify how the voltage loss is governed in fullerene and nonfullerene OSCs. The excitation fluence-dependent data of the QFLS and the V_{OC} of PM6:Y6 device reveal a negligible voltage loss due to recombination processes in and/or at the interface of the transport layers and the electrodes. Without the transport layers, however, 453 meV is lost due to surface recombination. Furthermore, in these devices, we observe no saturation effects of the V_{OC} or the QFLS, excluding any thermal effects in the devices. Our results clearly show that while the good choice of selective transport layers minimizes surface recombination losses, the recombination channels in the bulk are needed to be eliminated to improve the performance of PM6:Y6 solar cells. This work demonstrates how surface recombination losses can be unambiguously identified and suppressed.

Supporting Information

Supporting Information is available from the Wiley Online Library or from the author.

Acknowledgements

The authors acknowledge the Alexander von Humboldt Foundation for funding. H.Y.W. acknowledges financial support from the National Research Foundation (NRF) of Korea (2019R1A2C2085290 and 2019R1A6A1A11044070). O.J.S. acknowledges support from the Sêr Cymru Program through the European Regional Development Fund, Welsh European Funding Office, and Swansea University strategic initiative in Sustainable Advanced Materials. The authors thank Bowen Sun for partly preparing the studied devices. Open access funding enabled and organized by Projekt DEAL.

Conflict of Interest

The authors declare no conflict of interest.

Keywords

nonfullerene acceptors, organic solar cells, quasi-Fermi level splitting, quasi-steady-state photoinduced absorptions, surface recombinations, voltage losses

Received: October 13, 2020
Revised: November 5, 2020
Published online: November 19, 2020

[1] C. Yan, S. Barlow, Z. Wang, H. Yan, A. K. Y. Jen, S. R. Marder, X. Zhan, *Nat. Rev. Mater.* **2018**, *3*, 1.
[2] J. Zhang, H. S. Tan, X. Guo, A. Facchetti, H. Yan, *Nat. Energy* **2018**, *3*, 720.
[3] J. Hou, O. Inganas, R. H. Friend, F. Gao, *Nat. Mater.* **2018**, *17*, 119.
[4] J. Yuan, Y. Zhang, L. Zhou, G. Zhang, H. L. Yip, T. K. Lau, X. Lu, C. Zhu, H. Peng, P. A. Johnson, M. Leclerc, Y. Cao, J. Ulanski, Y. Li, Y. Zou, *Joule* **2019**, *3*, 1140.

[5] Y. Cui, H. Yao, J. Zhang, T. Zhang, Y. Wang, L. Hong, K. Xian, B. Xu, S. Zhang, J. Peng, Z. Wei, F. Gao, J. Hou, *Nat. Commun.* **2019**, *10*, 1.
[6] Q. Liu, Y. Jiang, K. Jin, J. Qin, J. Xu, W. Li, J. Xiong, J. Liu, Z. Xiao, K. Sun, S. Yang, X. Zhang, L. Ding, *Sci. Bull.* **2020**, *65*, 272.
[7] L. Perdigón-Toro, H. Zhang, A. Markina, J. Yuan, S. M. Hosseini, C. M. Wolff, G. Zuo, M. Stolterfoht, Y. Zou, F. Gao, D. Andrienko, S. Shoaee, D. Neher, *Adv. Mater.* **2020**, *32*, 1906763.
[8] T. Kirchartz, U. Rau, *Phys. Status Solidi Appl. Mater. Sci.* **2008**, *205*, 2737.
[9] J. Liu, S. Chen, D. Qian, B. Gautam, G. Yang, J. Zhao, J. Bergqvist, F. Zhang, W. Ma, H. Ade, O. Inganäs, K. Gundogdu, F. Gao, H. Yan, *Nat. Energy* **2016**, *1*, 1.
[10] D. Baran, T. Kirchartz, S. Wheeler, S. Dimitrov, M. Abdelsamie, J. Gorman, R. S. Ashraf, S. Holliday, A. Wadsworth, N. Gasparini, P. Kaienburg, H. Yan, A. Amassian, C. J. Brabec, J. R. Durrant, I. McCulloch, *Energy Environ. Sci.* **2016**, *9*, 3783.
[11] D. Qian, Z. Zheng, H. Yao, W. Tress, T. R. Hopper, S. Chen, S. Li, J. Liu, S. Chen, J. Zhang, X. K. Liu, B. Gao, L. Ouyang, Y. Jin, G. Pozina, I. A. Buyanova, W. M. Chen, O. Inganäs, V. Coropceanu, J. L. Bredas, H. Yan, J. Hou, F. Zhang, A. A. Bakulin, F. Gao, *Nat. Mater.* **2018**, *17*, 703.
[12] S. Li, L. Zhan, C. Sun, H. Zhu, G. Zhou, W. Yang, M. Shi, C. Z. Li, J. Hou, Y. Li, H. Chen, *J. Am. Chem. Soc.* **2019**, *141*, 3073.
[13] J. Yuan, T. Huang, P. Cheng, Y. Zou, H. Zhang, J. L. Yang, S. Y. Chang, Z. Zhang, W. Huang, R. Wang, D. Meng, F. Gao, Y. Yang, *Nat. Commun.* **2019**, *10*, 1.
[14] T. Kirchartz, F. Deledalle, P. S. Tuladhar, J. R. Durrant, J. Nelson, *J. Phys. Chem. Lett.* **2013**, *4*, 2371.
[15] S. Wheeler, F. Deledalle, N. Tokmoldin, T. Kirchartz, J. Nelson, J. R. Durrant, *Phys. Rev. Appl.* **2015**, *4*, 024020.
[16] I. Zonno, B. Krogmeier, V. Katte, D. Lübke, A. Martinez-Otero, T. Kirchartz, *Appl. Phys. Lett.* **2016**, *109*, 183301.
[17] K. Tvingstedt, L. Gil-Escrig, C. Momblona, P. Rieder, D. Kiermasch, M. Sessolo, A. Baumann, H. J. Bolink, V. Dyakonov, *ACS Energy Lett.* **2017**, *2*, 424.
[18] J. P. Correa-Baena, W. Tress, K. Domanski, E. H. Anaraki, S. H. Turren-Cruz, B. Roose, P. P. Boix, M. Grätzel, M. Saliba, A. Abate, A. Hagfeldt, *Energy Environ. Sci.* **2017**, *10*, 1207.
[19] A. Phys, A. Azeez, A. Azeez, **2020**, *043302*, 043302.
[20] E. L. Ratcliff, B. Zacher, N. R. Armstrong, *J. Phys. Chem. Lett.* **2011**, *2*, 1337.
[21] W. Shockley, *Bell Syst. Tech. J.* **1949**, *28*, 435.
[22] P. Würfel, W. Ruppel, *J. Phys. C Solid State Phys.* **1982**, *15*, 3967.
[23] K. Schick, E. Daub, S. Finkbeiner, P. Würfel, *Appl. Phys. A Solids Surf.* **1992**, *54*, 109.
[24] E. Daub, P. Würfel, *Phys. Rev. Lett.* **1995**, *74*, 1020.
[25] P. Caprioglio, M. Stolterfoht, C. M. Wolff, T. Unold, B. Rech, S. Albrecht, D. Neher, *Adv. Energy Mater.* **2019**, *9*, 1901631.
[26] I. L. Braly, D. W. Dequilettes, L. M. Pazos-Outón, S. Burke, M. E. Ziffer, D. S. Ginger, H. W. Hillhouse, *Nat. Photonics* **2018**, *12*, 355.
[27] M. Stolterfoht, C. M. Wolff, J. A. Márquez, S. Zhang, C. J. Hages, D. Rothhardt, S. Albrecht, P. L. Burn, P. Meredith, T. Unold, D. Neher, *Nat. Energy* **2018**, *3*, 847.
[28] M. Stolterfoht, P. Caprioglio, C. M. Wolff, J. A. Márquez, J. Nordmann, S. Zhang, D. Rothhardt, U. Hörmann, Y. Amir, A. Redinger, L. Kegelmann, F. Zu, S. Albrecht, N. Koch, T. Kirchartz, M. Saliba, T. Unold, D. Neher, *Energy Environ. Sci.* **2019**, *12*, 2778.
[29] C. M. Wolff, P. Caprioglio, M. Stolterfoht, D. Neher, *Adv. Mater.* **2019**, *31*, 1902762.
[30] G. D. Scholes, G. Rumbles, *Nat. Mater.* **2006**, *5*, 683.
[31] A. Armin, J. R. Durrant, S. Shoaee, *J. Phys. Chem. C* **2017**, *121*, 13969.
[32] J. Benduhn, K. Tvingstedt, F. Piersimoni, S. Ullbrich, Y. Fan, M. Tropiano, K. A. McGarry, O. Zeika, M. K. Riede, C. J. Douglas, S. Barlow, S. R. Marder, D. Neher, D. Spoltore, K. Vandewal, *Nat. Energy* **2017**, *2*, 17053.
[33] S. Shoaee, A. Armin, M. Stolterfoht, S. M. Hosseini, J. Kurpiers, D. Neher, *Sol. RRL* **2019**, *3*, 1900184.
[34] R. Schueppel, K. Schmidt, C. Uhrich, K. Schulze, D. Wynands, J. L. Brédas, B. Maennig, M. Pfeiffer, K. Leo, E. Brier, E. Reinold, H.-B. Bu, P. Baeuerle, *Proc. of SPIE* **2007**, *6656*, 66560G.
[35] N. M. Wilson, S. Sandén, O. J. Sandberg, R. Österbacka, *J. Appl. Phys.* **2017**, *121*, 095701.
[36] L. Q. Phuong, S. M. Hosseini, C. W. Koh, H. Y. Woo, S. Shoaee, *J. Phys. Chem. C* **2019**, *123*, 27417.
[37] R. Coehoorn, W. F. Pasveer, P. A. Bobbert, M. A. J. Michels, *Phys. Rev. B Condens. Matter Mater. Phys.* **2005**, *72*, 155206.
[38] P. G. Brown, H. Sirringhaus, M. Harrison, M. Shkunov, R. H. Friend, *Phys. Rev. B Condens. Matter Mater. Phys.* **2001**, *63*, 125204.
[39] E. Collado-Fregoso, S. N. Hood, S. Shoaee, B. C. Schroeder, I. McCulloch, I. Kassal, D. Neher, J. R. Durrant, *J. Phys. Chem. Lett.* **2017**, *8*, 4061.
[40] S. Shoaee, M. P. Eng, E. Espíldora, J. L. Delgado, B. Campo, N. Martín, D. Vanderzande, J. R. Durrant, *Energy Environ. Sci.* **2010**, *3*, 971.
[41] O. J. Sandberg, M. Nyman, R. Österbacka, *Phys. Rev. Appl.* **2014**, *1*, 024003.
[42] U. Rau, B. Blank, T. C. M. Müller, T. Kirchartz, *Phys. Rev. Appl.* **2017**, *7*, 044016.
[43] L. Krückemeier, U. Rau, M. Stolterfoht, T. Kirchartz, *Adv. Energy Mater.* **2020**, *10*, 1902573.
[44] N. Tokmoldin, S. M. Hosseini, M. Raoufi, L. Q. Phuong, O. J. Sandberg, H. Guan, Y. Zou, D. Neher, S. Shoaee, *J. Mater. Chem. A* **2020**, *8*, 7854.
[45] O. J. Sandberg, A. Armin, *Synth. Met.* **2019**, *254*, 114.
[46] O. J. Sandberg, A. Sundqvist, M. Nyman, R. Österbacka, *Phys. Rev. Appl.* **2016**, *5*, 044005.
[47] A. Karki, J. Vollbrecht, A. L. Dixon, N. Schopp, M. Schrock, G. N. M. Reddy, T. Q. Nguyen, *Adv. Mater.* **2019**, *31*, 1903868.